Biomaterials 34 (2013) 9264–9277

Contents lists available at ScienceDirect

Biomaterials

journal homepage: www.elsevier.com/locate/biomaterials

Cytocompatibility, osseointegration, and bioactivity of three-dimensional porous and nanostructured network on polyetheretherketone

Ying Zhao [a,b,1], Hoi Man Wong [a,1], Wenhao Wang [a,b], Penghui Li [b], Zushun Xu [b,c], Eva Y.W. Chong [a], Chun Hoi Yan [a,d], Kelvin W.K. Yeung [a,d,*], Paul K. Chu [b,**]

[a] Department of Orthopaedics & Traumatology, The University of Hong Kong, Pokfulam Road, Hong Kong, China
[b] Department of Physics and Materials Science, City University of Hong Kong, Tat Chee Avenue, Kowloon, Hong Kong, China
[c] Ministry-of-Education Key Laboratory for the Green Preparation and Application of Functional Materials, College of Materials Science and Engineering, Hubei University, Wuhan 430062, China
[d] Shenzhen Key Laboratory for Innovative Technology in Orthopaedic Trauma, The University of Hong Kong Shenzhen Hospital, 1 Haiyuan 1st Road, Futian District, Shenzhen, China

ARTICLE INFO

Article history:
Received 30 July 2013
Accepted 21 August 2013
Available online 14 September 2013

Keywords:
Polyetheretherketone
Biocompatibility
Osseointegration
Surface modification
Interface
Bioactivity

ABSTRACT

Porous biomaterials with the proper three-dimensional (3D) surface network can enhance biological functionalities especially in tissue engineering, but it has been difficult to accomplish this on an important biopolymer, polyetheretherketone (PEEK), due to its inherent chemical inertness. In this study, a 3D porous and nanostructured network with bio-functional groups is produced on PEEK by sulfonation and subsequent water immersion. Two kinds of sulfonation-treated PEEK (SPEEK) samples, SPEEK-W (water immersion and rinsing after sulfonation) and SPEEK-WA (SPEEK-W with further acetone rinsing) are prepared. The surface characteristics, *in vitro* cellular behavior, *in vivo* osseointegration, and apatite-forming ability are systematically investigated by X-ray photoelectron spectroscopy, Fourier-transform infrared spectroscopy, scanning electron microscopy, cell adhesion and cell proliferation assay, real-time RT-PCR analysis, micro-CT evaluation, push-out tests, and immersion tests. SPEEK-WA induces pre-osteoblast functions including initial cell adhesion, proliferation, and osteogenic differentiation *in vitro* as well as substantially enhanced osseointegration and bone-implant bonding strength *in vivo* and apatite-forming ability. Although SPEEK-W has a similar surface morphology and chemical composition as SPEEK-WA, its cytocompatibility is inferior due to residual sulfuric acid. Our results reveal that the pre-osteoblast functions, bone growth, and apatite formation on the SPEEK surfaces are affected by many factors, including positive effects introduced by the 3D porous structure and SO_3H groups as well as negative ones due to the low pH environment. Surface functionalization broadens the use of PEEK in orthopedic implants.

1. Introduction

Metallic biomaterials such as titanium alloys have been widely used in orthopedic implants due to their excellent corrosion resistance, high mechanical strength, as well as cytocompatibility [1]. However, there are concerns regarding potential metal ion release and mismatched mechanical properties between the metals and human bones. In fact, serious post-operative complications such as osteolysis, allergenicity, and loosening as well as eventual implant failure may occur [2]. To overcome these limitations and minimize negative post-implantation biological reactions, substitutes for metals are extensively pursued. One of the promising alternative materials is polyetheretherketone (PEEK) which has good chemical resistance, radiolucency, and mechanical properties similar to those of human bones [3–8]. Besides, it can be repeatedly sterilized and shaped by machining and heat contouring to fit the shape of bones [9]. In spite of these excellent attributes, the chemical and biological inertness of PEEK tends to limit bone fixation [3] and consequently, there have been efforts to incorporate hydroxyapatite (HA) into PEEK or deposit an HA coating on PEEK to

* Corresponding author. Department of Orthopaedics & Traumatology, The University of Hong Kong, Pokfulam Road, Hong Kong, China. Tel.: +852 22554654; fax: +852 28174392.
** Corresponding author. Tel.: +852 34427724; fax: +852 34420542.
E-mail addresses: wkkyeung@hku.hk (K.W.K. Yeung), paul.chu@cityu.edu.hk (P.K. Chu).
[1] The authors share the co-first authorship.

0142-9612/$ – see front matter © 2013 Elsevier Ltd. All rights reserved.
http://dx.doi.org/10.1016/j.biomaterials.2013.08.071

enhance bone-implant integration [10–15]. Nonetheless, the mechanical properties of the modified PEEK materials are compromised due to the poor physical bonding between PEEK and HA. Another strategy to improve the PEEK-bone interaction is to introduce porosity to PEEK. Based on the clinical outcome and histological evidence from retrieved implants, a porous surface can promote ingrowth of soft and hard tissue into the materials, thereby creating more biological anchorage to improve the stability of the implant [16]. Many techniques have hitherto been utilized to fabricate porous structures on metal surfaces, including machining, shotblasting, anodic oxidation, alkali treatment and acid-etching [17]. However, the related work on PEEK is relatively scarce due to its inherent chemical resistance and consequently, the proper porous surface structure has not yet been realized.

Sulfonation treatment produces a proton exchange membrane exhibiting excellent proton conductivity and this process has been primarily used in fuel cells [18–20]. By taking advantage of the etching action by concentrated sulfuric acid on PEEK during sulfonation, a porous network is produced on the PEEK samples. This technique has the advantages such as simple operation and non-light-of-sight characteristics, thus boding well for biomedical implants with a complex geometric shape. In this work, we also systematically evaluate the biofunctionalities of the sulfonated PEEK (SPEEK) with the three-dimensional (3D) porous and nano-structured network *in vitro* and *in vivo*. The mechanisms underlying the biocompatibility and bioactivity enhancement are proposed and discussed.

2. Materials and methods

2.1. Sample preparation

Medical grade PEEK (Ketron LSG, Quadrant EPP, USA) materials were used in this study. Disk samples with dimensions of Φ5 x 2 mm^3 were prepared for surface characterization, immersion tests and *in vitro* studies on 96-well tissue culture plates while disk samples with dimensions of Φ14 × 2 mm^3 were prepared for *in vitro* studies performed on 24-well tissue culture plates. The rod samples for *in vivo* animal studies were 2 mm in diameter and 6 mm long. All the samples were mechanically polished to a mirror finish and ultrasonically washed in acetone and ethanol. The fabrication process is schematically illustrated in Fig. 1. In order to obtain a uniform porous structure, supersonic stirring was utilized almost throughout the entire process. Sulfonation was conducted in supersonically stirred sulfuric acid (95–98 wt%, Aldrich Chemical Corp) at room temperature for 5 min. The samples were subsequently taken out and immersed in supersonically stirred distilled water. Afterwards, the samples were rinsed repeatedly with distilled water. Some of the SPEEK samples were dried (labeled as SPEEK-W) and the others were further rinsed with acetone followed by cleaning with distilled water and drying (labeled as SPEEK-WA).

2.2. Surface characterization

Field-emission scanning electron microscopy (FE-SEM, Leo 1530 FEG, Oxford) was employed to observe the surface topography of the prepared specimens. The average pore size was determined using the CTAn program (Skyscan Company, Belgium). The surface hydrophilicity of the specimens was assessed by water contact angle measurements performed on a Ramé-Hart (USA) instrument at ambient humidity and temperature. Fourier transform infrared (FTIR) spectra were recorded on the Equinoxss/Hyperion2000 manufactured by Bruker equipped with the attenuated total reflection (ATR) accessory. X-ray photoelectron spectroscopy (XPS, Physical electronics PHI 5802) with monochromatic Al K_α radiation source was employed to determine the chemical states. The binding energies were referenced to the C 1s line at 285.0 eV and a Gaussian–Lorentzian peak fitting model was adopted to deconvolute the S2p spectra.

2.3. In vitro studies

2.3.1. Cell culture

Mouse MC3T3-E1 pre-osteoblasts provided by the Royal Children's Hospital Melbourne were cultivated in a complete cell culture medium comprising a mixture of Dulbecco's modified eagle medium (DMEM, Gibco) and 10% fetal bovine serum (FBS, Gibco) in a humidified atmosphere of 5% CO_2 at 37 °C. Before cell culturing, all the samples were sterilized with 70% alcohol for 40 min and rinsed with sterile phosphate buffered saline (PBS) thrice. The medium for cell culture was refreshed every 3 days.

2.3.2. Cell adhesion

In the cell adhesion assay, MC3T3-E1 pre-osteoblasts were seeded on each sample in 96-well tissue culture plates at a density of 1×10^4 cells per well and cultured for 4 h. Afterwards, the seeded samples were rinsed twice with PBS and fixed with 2% polyoxymethylene. The nuclei were stained with Hoechst33342 (Sigma) and examined by fluorescence microscopy (Axio Observer, Carl Zeiss). The cytoskeleton protein F-actin was stained with phalloidin fluorescein isothiocyanate (Sigma) and observed by laser confocal scanning microscope (Leica SPE).

2.3.3. Cell viability and cell proliferation

The MTT assay was employed to quantitatively determine the viable MC3T3-E1 pre-osteoblasts on the samples [21]. 150 μl of the cell suspension were seeded on each sample on the 96-well tissue culture plates at a density of 5×10^3 cells/well and cultured in DMEM with 10% FBS for 1, 3, 7, and 14 days. At every prescribed time point, the specimens were gently rinsed twice with PBS and transferred to a new 96-well plate. After adding the MTT solution prepared by adding thiazolyl blue tetrazolium bromide (Sigma) powder to PBS, the specimens were incubated at 37 °C to form formazen which was dissolved using dimethyl sulfoxide. The absorbance was determined at 570 nm using a spectrophotometry (Biotek, USA).

Cell proliferation on the samples was studied by using the BrdU incorporation ELISA kit (Roche, US). The MC3T3-E1 pre-osteoblasts were seeded on each sample on 96-well tissue culture plates and cultured for 1, 3, 7, and 14 days. At the prescribed time points, the cells were labeled with the BrdU solution for 4 h. Afterwards, the cells were fixed for 30 min at room temperature and incubated with the anti-BrdU-POD solution for 2 h. The substrate solution was applied after several rising with PBS. The reaction was stopped by 1 M H_2SO_4 and the absorbance was recorded by the multimode detector on the Thermo Scientific MULTISKAN GO at a wavelength of 450 nm.

2.3.4. Cell apoptosis

Flow cytometry was performed for simultaneous detection of necrosis and apoptosis of cells. The samples were placed on a 24-well tissue culture plate and 5×10^4 cells/cm^2 MC3T3-E1 pre-osteoblasts were seeded on each sample and cultured for 1 and 3 days. At the respective time points, the cells were harvested and the cell density was adjusted to 2.5×10^5 cells/ml using a binding buffer. Afterwards, the cells were re-suspended in 200 μl of the buffer containing 5 μl Annexin V-FITC and incubated at room temperature for 30 min. The resulting cells were re-

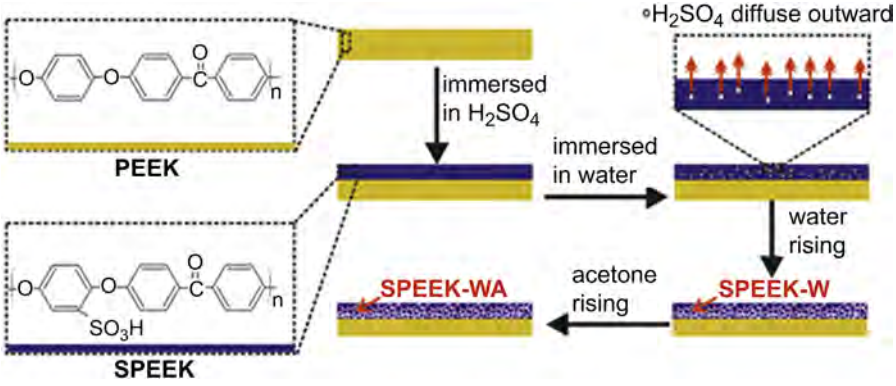

Fig. 1. Schematic diagram of the fabrication process on the 3D porous SPEEK-W and SPEEK-WA samples.

Table 1
Primer pairs used in real-time PCR analysis.

Gene	Forward primer	Reverse primer
Gapdh	5′-ACCCAGAAGACTGTGGATGG-3′	5′-CACATTGGGGGTAGGAACAC-3′
ALP	5′-CCAGCAGGTTTCTCTCTTGG-3′	5′-GGGATGGAGGAGAGAAGGTC-3′
Col1a1	5′-GAGCGGAGAGTACTGGATCG-3′	5′-GTTCGGGCTGATGTACCAGT-3′
Runx2	5′-CCCAGCCACCTTTACCTACA-3′	5′-TATGGAGTGCTGCTGGTCTG-3′

suspended in 200 μl of the buffer containing 10 μl PI after washing several times and finally, the cells were filtered and analyzed by flow cytometry (BD FACSCanto II Analyzer).

2.3.5. Osteogenic gene expression monitored by quantitative real-time RT-PCR

The expression of osteogenesis-related genes was analyzed using the real-time reverse-transcriptase polymerase chain reaction (Real-time RT-PCR). MC3T3-E1 pre-osteoblasts with a density of 2.5×10^4 cells/well were seeded and cultured for 3, 7 and 14 days. The total RNA was isolated with the TRIZOL reagent (Invitrogen, USA) and the complementary DNA (cDNA) was reverse-transcribed from 1 μg of total RNA using Superscript III (Invitrogen, USA). The forward and reverse primers for the selected genes are listed in Table 1. The expressions of the osteogenesis-related genes, including alkaline phosphatase (ALP), runt-related transcription factor 2 (*Runx2*) and Type I collagen alpha 1 (*Col1a1*), were quantified using Real-time PCR (ABI prism 7900HT sequence detection system) with SYBR Green PCR Master Mix (Applied Biosystems, USA). The relative mRNA expression level of each gene was normalized with the house-keeping gene glyceraldehyde-3-phosphate dehydrogenase (GAPDH) and determined by the Ct values.

2.4. In vivo animal studies

2.4.1. Surgery

The animal experiments were approved by the Department of Health and the Committee on the Use of Live Animals in Teaching and Research (CULATR). Twenty

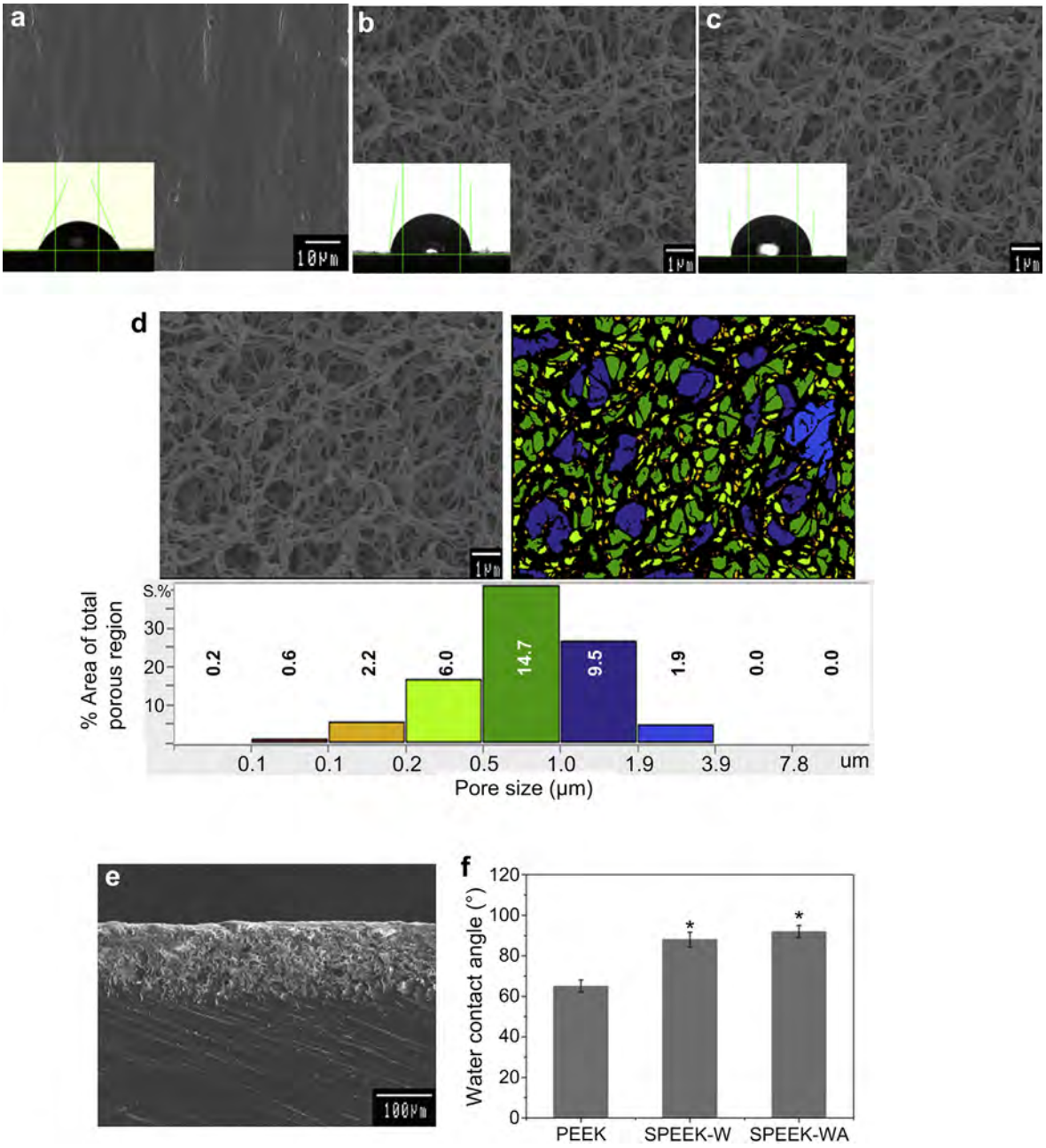

Fig. 2. FE-SEM photographs acquired from the surface of (a) PEEK control, (b) SPEEK-W, (c) SPEEK-WA with typical water droplet images inserted in the bottom left, (d) characterization of pores formed on the SPEEK-WA using CTAn software, (e) cross section of SPEEK, and (f) water contact angle of the samples measured by the static sessile drop method, *represents $p < 0.05$ compared to PEEK control.

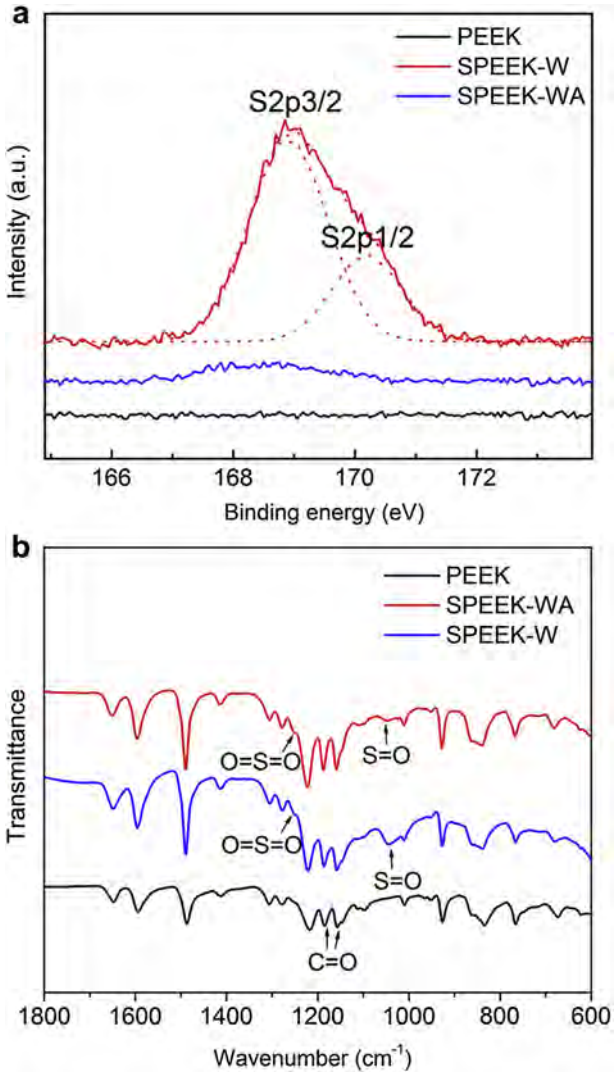

Fig. 3. Surface characterization of the PEEK, SPEEK-W and SPEEK-WA samples: (a) XPS S2p spectra: The dotted lines represent the S2p3/2 and S2p1/2 spectra deconvoluted by S2p spectrum using Gaussian–Lorentzian peak fitting model; (b) FTIR spectra: The appearance of the signal at 1255 cm^{-1} and 1050 cm^{-1} represents O=S=O dissymmetric stretching and S=O symmetric stretching, respectively.

seven 8-week old female Sprague Dawley (SD) rats from the Laboratory Animal Unit of the University of Hong Kong were used in this study. Their average weight was approximately 200 g. All the rats were randomly assigned to three groups corresponding to SPEEK-WA, SPEEK-W, and PEEK control. Before the surgery, the rats were anaesthetized with ketamine (20 mg/kg), xylazine (2 mg/kg) and buprenorphine (0.05 mg/kg). A hole 2 mm in diameter was prepared at the left or right distal femur of the rats using dental drill until the hole reached 6 mm in depth and the sample was then implanted into the prepared hole. After operation, the rats received subcutaneous injection of oxytetracycline (30 mg/kg) and ketoprofen (3 mg/kg) for 3 consecutive days. All the rats were sacrificed 8 weeks post-operation.

2.4.2. Micro-CT evaluation

After the operation, the rats underwent micro-computed tomography (Micro-CT) evaluation directly using a micro-computed tomography device (SKYSCAN 1076, Skyscan Company) and more micro-CT examinations were conducted every week up to week 8. After scanning, the two-dimensional (2D) and three-dimensional (3D) models were reconstructed using the NRecon (Skyscan Company) and CTVol (Skyscan Company, Belgium), and the bone volume around the implant was determined by the CTAn program (Skyscan Company, Belgium).

2.4.3. Histological evaluation

The bone samples (3 per group) with the implants were harvested and fixed in 10% buffered formalin for 3 days, dehydrated in a series of solutions with different ethanol concentrations of 70%, 80%, 90%, 99%, and 100% v/v for 3 days each, and transferred to a methylmethacrylate (Technovit 9100 New®, Heraeus Kulzer, Hanau, Germany) solution at 37 °C within 1 week. Afterwards, the embedded samples were cut into sections with a thickness of 50–70 μm. The sectioned samples were stained with Giemsa (MERCK, Germany) stain. The length of the bone in contact with the implant was determined according to the histological image and the percentage of bone-implant contact was calculated. Optical microscopy and scanning electron microscopy were conducted to observe bone ingrowth and integration with the host tissue. EDS (energy-dispersive X-ray spectroscopy) and elemental mapping were performed to determine the interface composition after 8 weeks of implantation.

2.4.4. Push-out test

To investigate the interface bonding between the bone and implant, push-out tests were performed on a biomechanical test apparatus (MTS 858.02 Mini Bionix system) (Supplementary Fig. S1). The bone samples with the implants were harvested 8 weeks post-operation and measured within 24 h after sacrificing the animals. The tests were performed at a loading rate of 1 mm/min. The load-deflection curves were recorded during the pushing period and the failure load was defined as the maximum load values. The push-out load was determined by averaging the results from six push-out tests.

2.5. Formation of bone-like apatite

The PEEK, SPEEK-W, and SPEEK-WA samples were immersed in a simulated body fluid (SBF) [22] (Na^+ 142.0, K^+ 5.0, Mg^{2+} 1.5, Ca^{2+} 2.5, Cl^- 147.8, HCO_3^- 4.2, HPO_4^{2-} 1.0, and SO_4^{2-} 0.5 mM and *pH* (7.4) nearly equal to that of human blood plasma) at 37 °C for 28 days to examine the bioactivity. After immersion, the specimens were gently rinsed with distilled water and ethanol and after drying, the surface deposits were examined by XPS. After sputter-coated with gold, the microstructure of specimens were characterized by SEM and energy dispersive spectrometry (EDS).

2.6. Statistical analysis

All the *in vitro* experiments were independently performed in triplicates and each data point represents three replicate measurements. The data were expressed as averages ± standard deviations. The results of the *in vitro* and *in vivo* experiments were statistically analyzed by the one-way analysis of variance (ANOVA) and a p value less than 0.05 was considered to be statistically significant.

3. Results

Fig. 2 shows the SEM photographs acquired from SPEEK samples and untreated PEEK control. After surface treatment, the originally smooth morphology (Fig. 2a) is altered and a 3D porous network is observed from SPEEK-W (Fig. 2b) and SPEEK-WA (Fig. 2c). These two processed samples have a similar surface morphology. As shown in Fig. 2d, most of the pores are between 0.5 μm and 1.0 μm in size according to the analysis by the CTAn software, suggesting a nanostructured surface (Fig. 2d). The thickness of the modified layer is about 100 μm (Fig. 2e). The hydrophilicity of the samples is evaluated by the static sessile drop method and the images of the water droplets on the samples are presented in the bottom left of the Fig. 2a–c. The measured water contact angles (CA_{water}) are summarized as a histogram in Fig. 2f and both SPEEK-W (CA_{water} = 88°) and SPEEK-WA (CA_{water} = 92°) are significantly more hydrophobic than the PEEK control (CA_{water} = 65°).

The XPS spectra in Fig. 3a reveal surface chemical variations after sulfonation. The two peaks at 168.1 and 169.2 eV correspond to 2p3/2 and 2p1/2 of sulfur with a high oxidation state, that is, SO_3H group [23]. There are more sulfur-containing groups on SPEEK-W compared to SPEEK-WA.

Fig. 3b shows the FTIR spectra acquired from the PEEK control, SPEEK-W, and SPEEK-WA. In the three spectra, all the characteristic bands are present, including the diphenylketone bands at 1650, 1490 and 926 cm^{-1}, C–O–C stretching vibration of the diaryl groups at 1188 and 1158 cm^{-1}, as well as a peak at 1600 cm^{-1} related to C=C in the benzene ring in PEEK [24]. The main structure of SPEEK and PEEK is similar. Closer examination reveals extra characteristic polymer bands from SPEEK such as O=S=O dissymmetric stretching at 1255 cm^{-1} and S=O symmetric stretching at 1050 cm^{-1} [25,26]. The data confirm that SO_3H

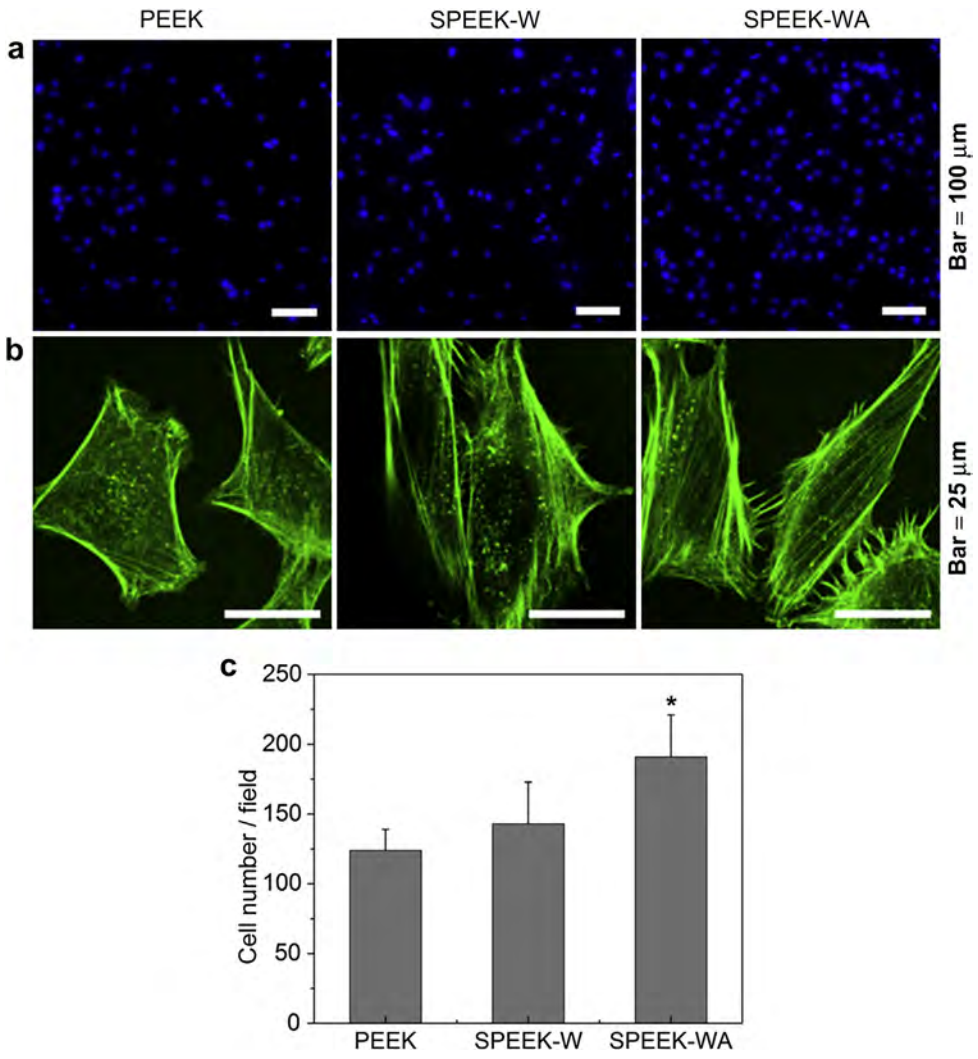

Fig. 4. MC3T3-E1 pre-osteoblast adhesion measured on the various samples after incubation for 4 h (a) nuclei in blue stained with Hoechst33342 and observed under a fluorescence microscope, (b) cytoskeleton in green stained with phalloidin fluorescein isothiocyanate and observed under a confocal scanning microscope, (c) pre-osteoblasts measured by counting cell nuclei under a fluorescence microscope. Statistical significance is indicated by $^{*}P < 0.05$ compared to PEEK control. (For interpretation of the references to color in this figure legend, the reader is referred to the web version of this article.)

functional groups are introduced to the PEEK surface by sulfonation.

The viable pre-osteoblasts adhered on the samples after incubation for 4 h are shown in Fig. 4. The cell morphology on SPEEK-WA and SPEEK-W is comparable to that on the PEEK control, but the adherent cell numbers on all the SPEEK samples are enhanced compared to the PEEK control. Among the SPEEK samples, SPEEK-WA shows higher initial cell adhesion than SPEEK-W.

Cell viability measured by the MTT assay is shown in Fig. 5a. Significantly increased cell viability can be observed on SPEEK-WA at every time point compared to SPEEK-W and PEEK control. In addition, the viable cell number on SPEEK-W is higher than that on the PEEK control, particularly at days 2, 4 and 14, revealing the improved cytocompatibility after treatment. Fig. 5b exhibits the fold change of BrdU incorporation after culturing for 1, 3, 7, and 14 days. Significantly enhanced BrdU incorporation is found from the SPEEK-W and SPEEK-WA samples throughout the culturing period compared to the PEEK control, suggesting that the proliferation rate of the cells on the treated samples is higher than that on the untreated PEEK control. Moreover, significantly higher BrdU incorporation is observed from the SPEEK-WA at day 1 and day 7 compared to SPEEK-W revealing that SPEEK-WA offers a more favorable cell environment for cell proliferation.

Fig. 6 shows the percentage of apoptotic cells and necrotic cells on the treated and untreated PEEK samples at the respective time points. No significant difference in the percentage of apoptotic cells can be observed from both the treated and untreated PEEK samples at day 1. However, a significantly higher percentage of apoptotic cells is found on the untreated sample at day 3 compared to the SPEEK samples, indicating that the SPEEK samples provide a more favorable environment for cells growth. Moreover, a significantly smaller percentage of necrotic cells is found from the SPEEK-WA sample at day 1, and no significant difference can be found between SPEEK-W and untreated PEEK thus revealing no harmful effect from the surface treatment.

The osteogenic differentiation properties are further assessed by quantitative real-time RT-PCR of ALP, *Runx2*, and *Col1a1* mRNA expression (Fig. 7). In general, the pre-osteoblasts cultured on SPEEK-WA exhibit the highest gene expressions followed by SPEEK-W. The PEEK control shows the least at every time point. Significant higher ($p < 0.05$) *Runx2*, ALP, and *Col1a1* expressions are found on SPEEK-W and SPEEK-WA at day 3 than the PEEK control. The ALP

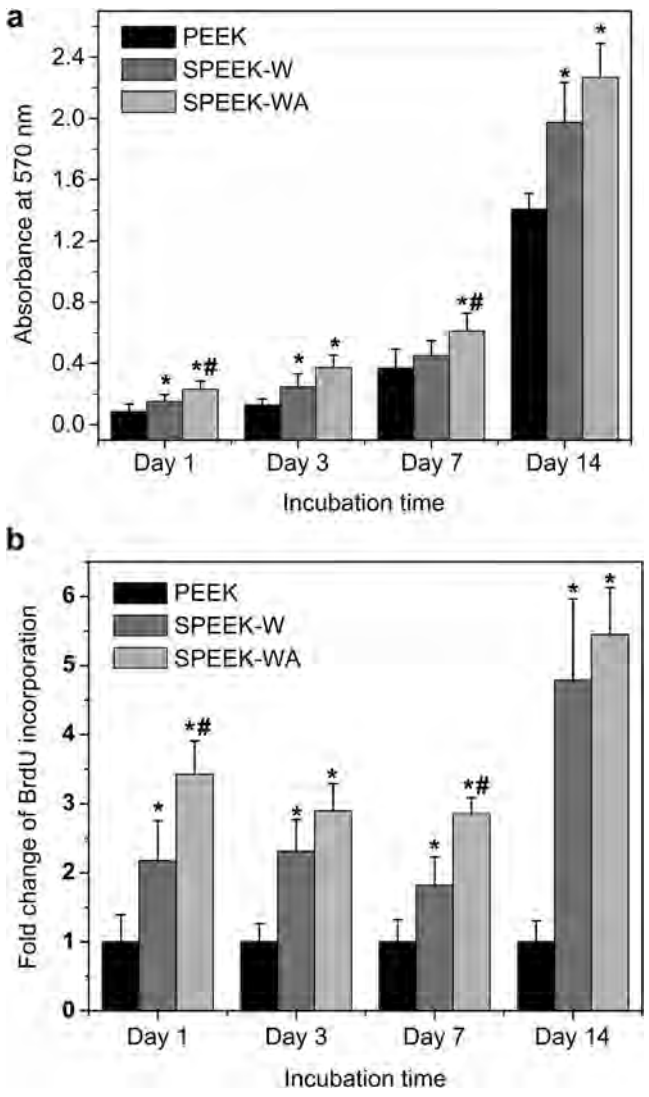

Fig. 5. Cell viability and cell proliferation of MC3T3-E1 pre-osteoblasts cultured on the SPEEK-WA, SPEEK-W and PEEK control for 1, 3, 7 and 14 days: (a) Cell viability measured by the MTT assay; (b) Cell proliferation evaluated by the fold change of the incorporation of BrdU on samples. The data are normalized to the initially adherent cell number or BrdU incorporation. Statistical significance is indicated by $^{*}P < 0.05$ compared with PEEK control and $\#P < 0.05$ compared to SPEEK-W.

and *Col1a1* expressions on SPEEK-WA are dramatically higher than those on SPEEK-W and PEEK control at days 7 and 14. In addition, significant higher *Col1a1* expression is found on SPEEK-W at day 14 compared to the PEEK control.

New bone formation and implant change after operation are evaluated at prescribed time points by micro-CT. Fig. 8a shows the cross sections of the femur containing the implant 0, 1, 4, and 8 weeks after surgery. The corresponding percentage changes in the bone volume are shown in Fig. 8b. One week after surgery, more than 10% decrease in the bone volume is found on SPEEK-W, whereas there is an approximately 20% increase in the bone volume on SPEEK-WA. Two weeks after surgery, the bone volume on SPEEK-W increases to 102% and remains stable till week 8 and new bone formation on SPEEK-WA continuously increases to 153% after 8 weeks. In comparison to the PEEK control, there is approximately 20% increase in the bone volume on SPEEK-WA implant at week 8. During the whole implantation period, there is no apparent volume change in all the implants.

Fig. 9a–d shows the tissue response to the PEEK and SPEEK implants after 8 weeks using Giemsa staining. All the implants show direct contact with the newly formed bones. In particular, bone ingrowth can be observed from SPEEK-WA (Fig. 9d). It implies that the newly formed bone tissues penetrate into the porous surface layer and bond to the porous network of SPEEK. Hence, it is expected to lead to stronger adhesion to better sustain the implant. Osteoblasts, which are responsible for new bone formation, are also observed around the implants. More bones are found around the SPEEK-WA implants than PEEK control and SPEEK-W. Fig. 9e shows the percentage of bone-implant contact on the PEEK and SPEEK implants after week 8. There is more bone-implant contact on the SPEEK-WA implant in comparison with SPEEK-W and PEEK control. The results are consistent with the changes in the bone volume shown in Fig. 8b. SEM and EDS show that new bones bond to the SPEEK surface directly and extend to the porous structure and they contain calcium and phosphorus at a Ca/P ratio of about 1.66 (Fig. 10). There is experimental evidence that the porous structure on SPEEK favors osteoblast adhesion and bone ingrowth *in vivo*.

The results acquired from the push-out tests are shown in Fig. 11. The bonding strength between bone tissues and the various implants is different. The average maximum push-out loads obtained from PEEK, SPEEK-W and SPEEK-WA are 10.5, 47.1 and 54.9 N, respectively. It is obvious that materials with porous surfaces have higher bonding strength than smooth ones, suggesting a high level of mechanical interlocking between the implant and bones. Fig. 11b–d show the representative load-deflection curves of the PEEK, SPEEK-W and SPEEK-WA samples. A typical plateau appears from the SPEEK-WA curve as shown in Fig. 11d and it is related to the collapse of cells in the initial stage of loading [27]. As the load is continuously increased, a sharp peak occurs from the PEEK curve suggesting abrupt rupture between the bone and implant. In contrast, the SPEEK-WA and SPEEK-W curves show a zigzag pattern around the maximum load indicative of gradual rupture. In addition, different load progression can be observed from the load-deflection curve of SPEEK-WA and SPEEK-W. For example, when the effective deflection is extended to 0.3 mm, the push-out load of the interface between porous SPEEK-WA and bone increases to 13 N whereas it is 46 N for the porous SPEEK-W and bone.

Fig. 12 exhibits the surface morphology of the specimens after immersion in SBF for 28 days. A few scattered spherical particles can be observed from the untreated PEEK control. In contrast, the number of particles on SPEEK-W and SPEEK-WA is dramatically increased. The EDS spectra acquired from the immersed specimens reveal that the formed particle contain calcium and phosphorous and their ratio is about 1.50–1.66, which is approximately the same as that of the bone mineral. The XPS Ca2p and P2p spectra of the deposited spherical particles on SPEEK-WA immersed in SBF for 28 days are presented in Fig. 12e and f. The Ca2p spectrum exhibits a doublet at 347. 3 and 350.7 eV and the P2p spectrum shows a single peak at 133.0 eV, which are consistent with the published data for hydroxyapatite [28]. EDS, XPS, and SEM indicate that spherical particles formed on the sample surface after immersion in SBF for 28 days are composed of bone-like apatite and that sulfonation can significantly enhance the bioactivity.

4. Discussion

It is widely accepted that the initial interactions between the cells and implant surface are crucial to clinical success and improvement can lead to faster bone formation [29,30]. In this study, the incubation period of the seeded samples for pre-osteoblast adhesion is 4 h whereas the incubation times for pre-osteoblast proliferation are 2, 4, and 7 days. Both pre-osteoblast adhesion and proliferation are significantly enhanced on the

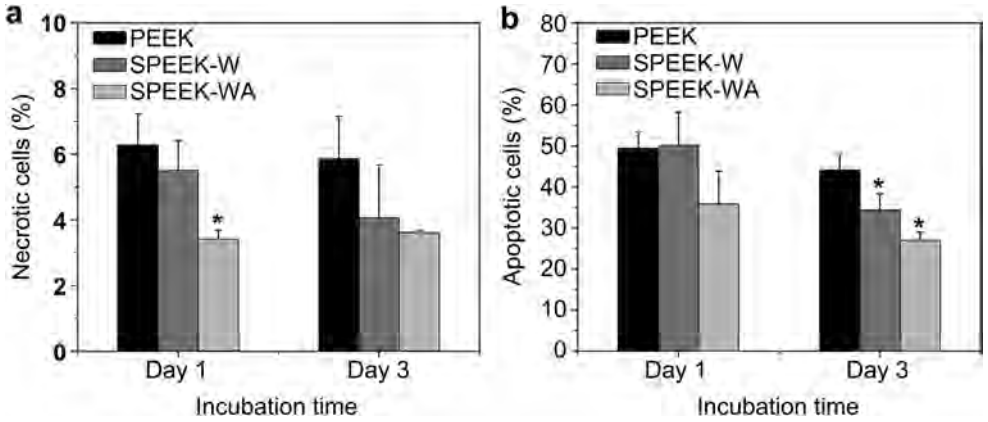

Fig. 6. Percentage of apoptosis cells and necrotic cells after culturing for 1 and 3 days with the statistical significance indicated by $^{*}P < 0.05$ compared to PEEK control.

nanostructured 3D porous SPEEK-WA compared to the PEEK control and no cytotoxic effects can be found from the MC3T3-E1 cells. Initial cell adhesion is usually responsible for the ensuing cell functions and eventual tissue integration, and cell proliferation is closely correlated with the amount of new bone formation. Hence, better pre-osteoblast adhesion and proliferation probably produce a larger mass of bone tissues around the implants and more robust bone-implant bonding is also expected *in vivo* [31,32].

The real-time RT-PCR results show that expressions of nearly all the genes, namely ALP, *Runx2* and *Col1a1*, are upregulated after sulfonation, particularly on SPEEK-WA. ALP is considered to be an early marker for osteogenic differentiation [33]. A higher ALP

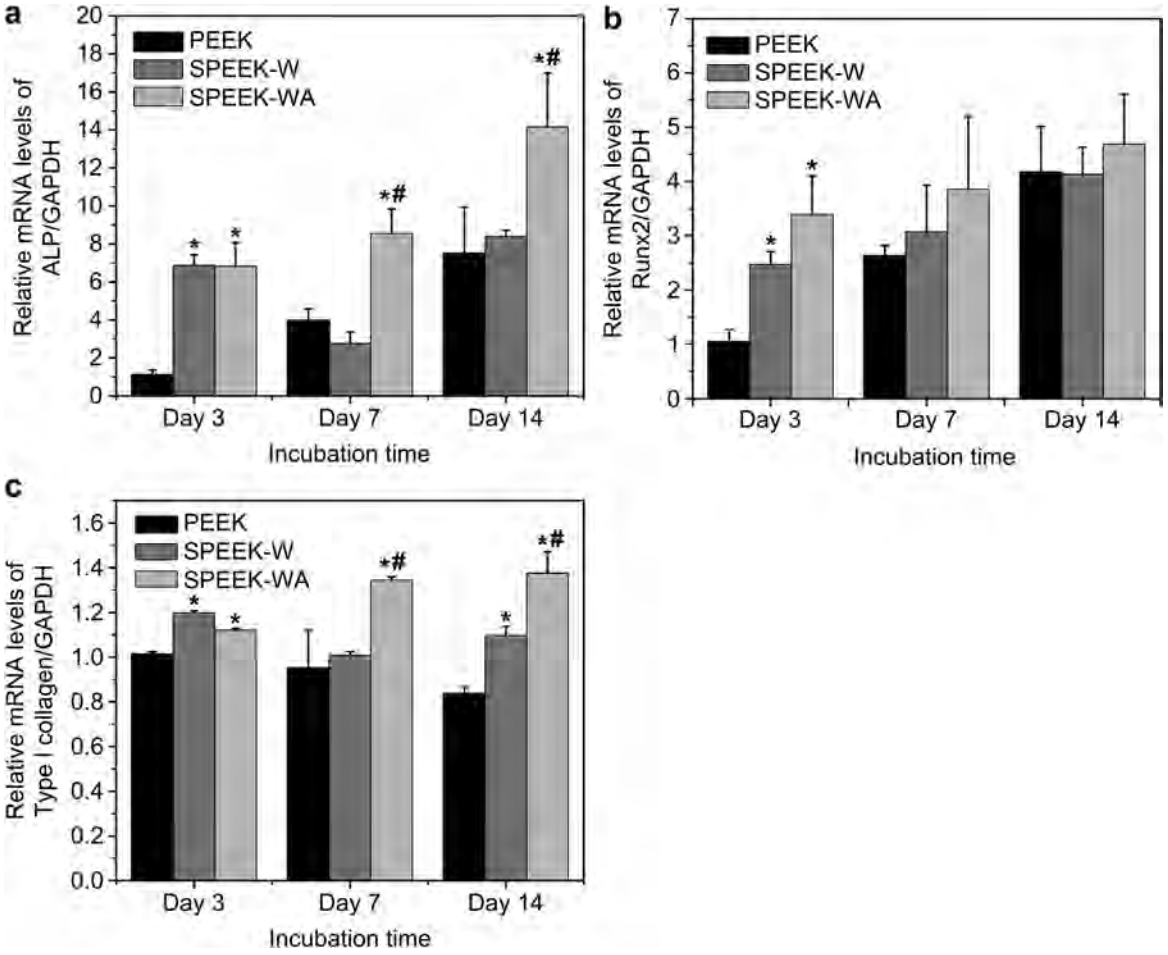

Fig. 7. Osteogenic differentiation by measuring the mRNA expression level of alkaline phosphatase (ALP), runt-related transcription factor 2 (Runx2) and type I collagen (Col1a1) after days 3, 7 and 14. The mRNA level is normalized to the house-keeping gene GAPDH. Statistical significance is indicated by $^{*}P < 0.05$ compared with PEEK control and $\#P < 0.05$ compared with SPEEK-W.

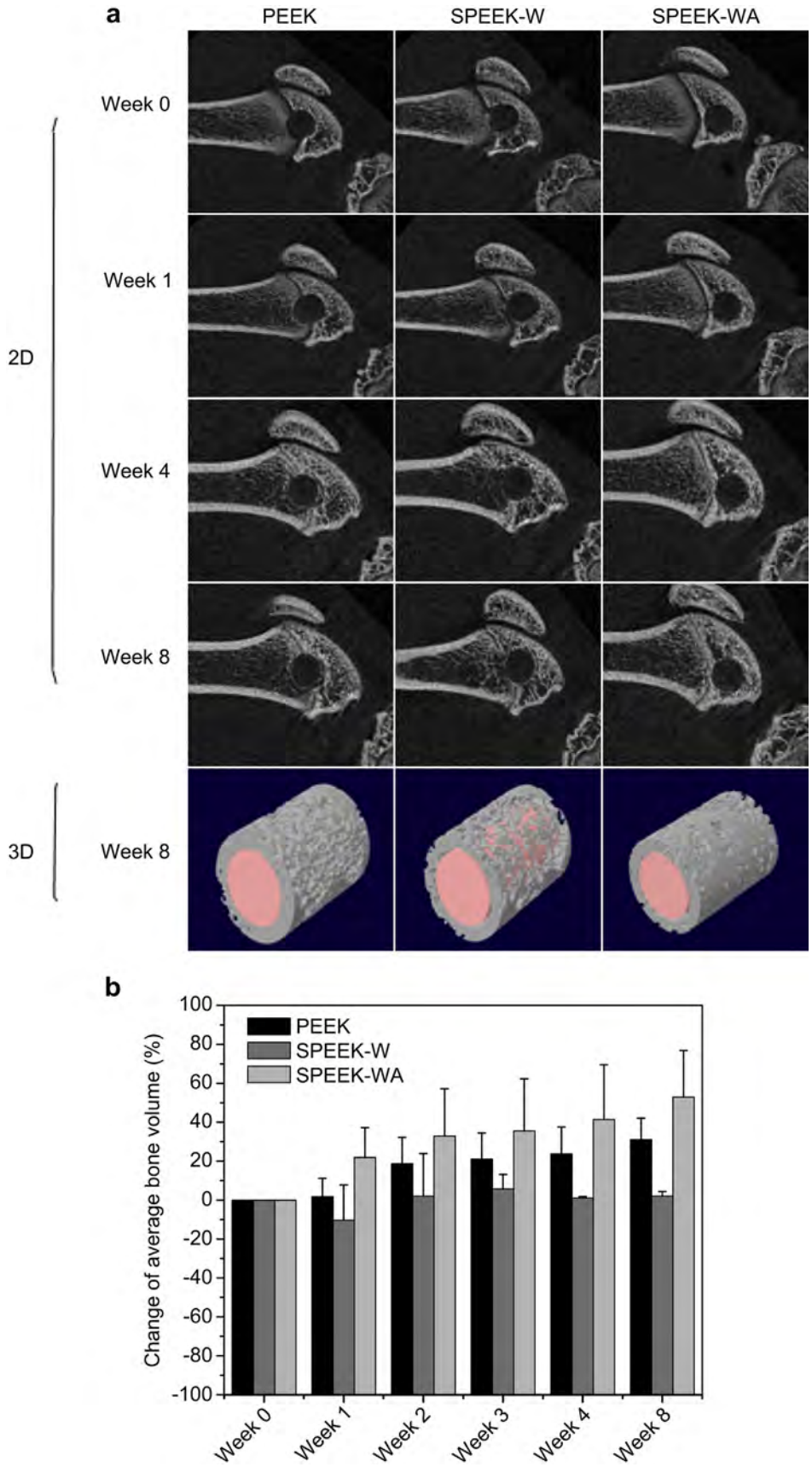

Fig. 8. Characterization of implants and the surrounding bones by Micro-CT: (a) Micro-CT 2D and 3D reconstruction models showing the status of the implants (pink in color) and bone (white in color) response 0, 1, 4, and 8 weeks after surgery; (b) Change of average bone volume around the implants 0, 1, 2, 3, 4, and 8 weeks after surgery. (For interpretation of the references to color in this figure legend, the reader is referred to the web version of this article.)

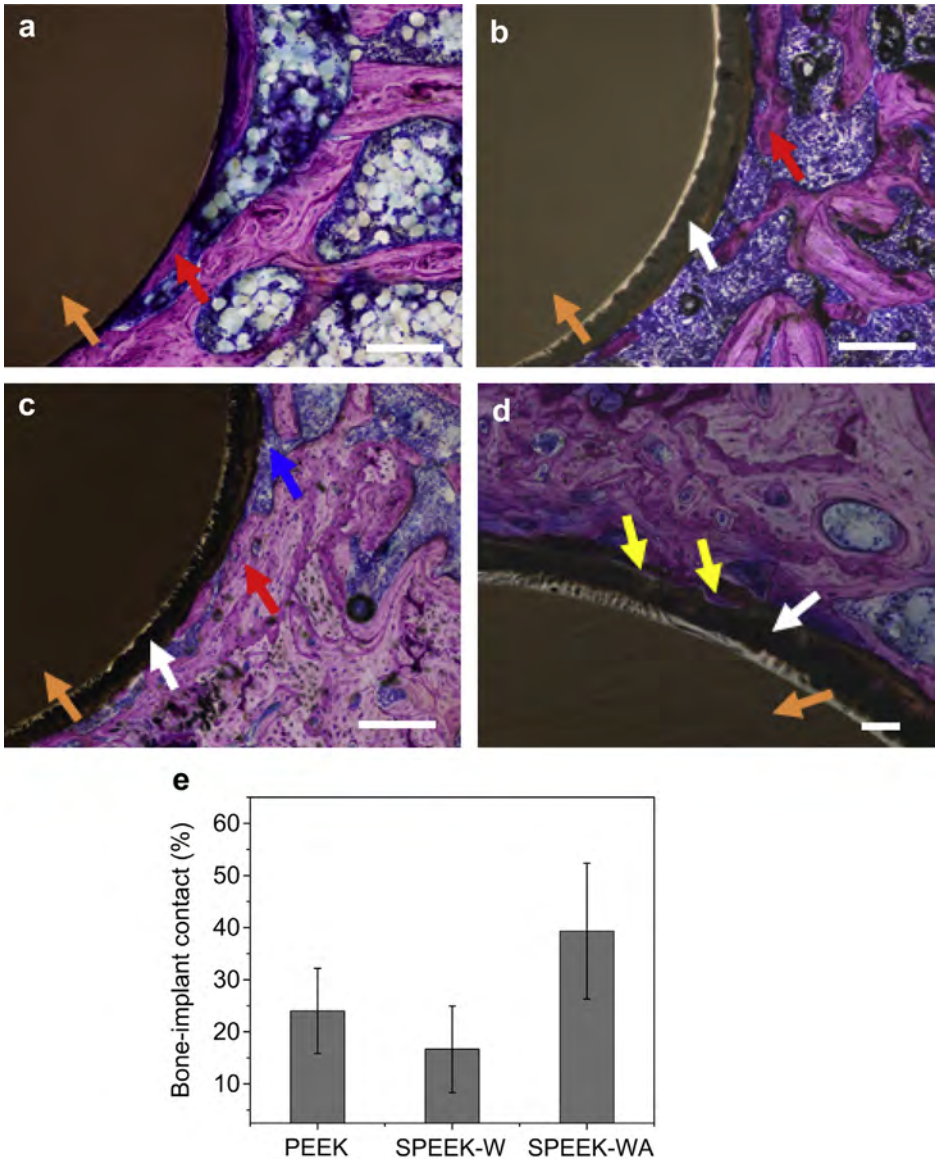

Fig. 9. Hard tissue sections of Giemsa stained around the implant after implantation for 8 weeks with the red arrows representing the newly formed bone, yellow arrows representing bone ingrowth, blue arrows representing osteoblasts, white arrows representing the SPEEK layer and orange arrows representing the PEEK substrate: (a) PEEK, (b) SPEEK-W, (c) SPEEK-A (low magnification) and (d) SPEEK-WA (high magnification). Scale bar is 200 μm. (e) Percentage of bone-implant contact on the PEEK, SPEEK-W and SPEEK-WA implant. (For interpretation of the references to color in this figure legend, the reader is referred to the web version of this article.)

expression of cells cultured on SPEEK indicates that it favors bone formation. Runx2 is the key transcription factor for osteoblastic differentiation [34,35] and no significant difference is found from the *Runx2* expression between SPEEK and control at days 7 and 14. However, a significantly higher expression can be detected at day 3, indicating that the porous SPEEK enhances osteoblastic differentiation in the early time points during cell culturing. *Col1a1* is the major components of extra cellular matrix deposition. The early and higher expression of *Col1a1* suggests that sulfonation can induce osteoblastic differentiation. Thus, with regard to osteogenic differentiation, the real-time RT-PCR also imparts the importance of SPEEK, especially SPEEK-WA.

The surface morphology plays an important role in the cytocompatibility of biomaterials, although the relationship between the morphology and biomedical behavior is still unclear [36–39]. In this study, a 3D porous and nanostructured network is produced by sulfonation and subsequent water immersion (see Fig. 1). It has been reported that sulfonation of PEEK occurs when the polymer is immersed in concentrated sulfuric acid at ambient temperature (Scheme 1) [40]. When the sample is taken out from the sulfuric acid, the formed SPEEK still swells and a small amount of sulfuric acid remains on the surface. After immersion in distilled water, SPEEK begins to morph from the swollen state to a solidified one. During the process, the excess sulfuric acid penetrates SPEEK and diffuses outward and so many pores are formed in the SPEEK layer during solidification. Furthermore, chemical introduction of SO_3H groups tailors chain conformation and packing of PEEK, destroys the original compact structure, and also promotes the formation of pores. It should be noted that the porous structure of SPEEK shows characteristics of a stretched 3D network, which may be related to hydrophilicity of SO_3H groups [41]. During water immersion, the hydrophilic SO_3H groups cause the polymer chain to continue swelling and consequently, a stretched 3D network is finally formed after the sulfuric acid is removed from SPEEK. Since acetone

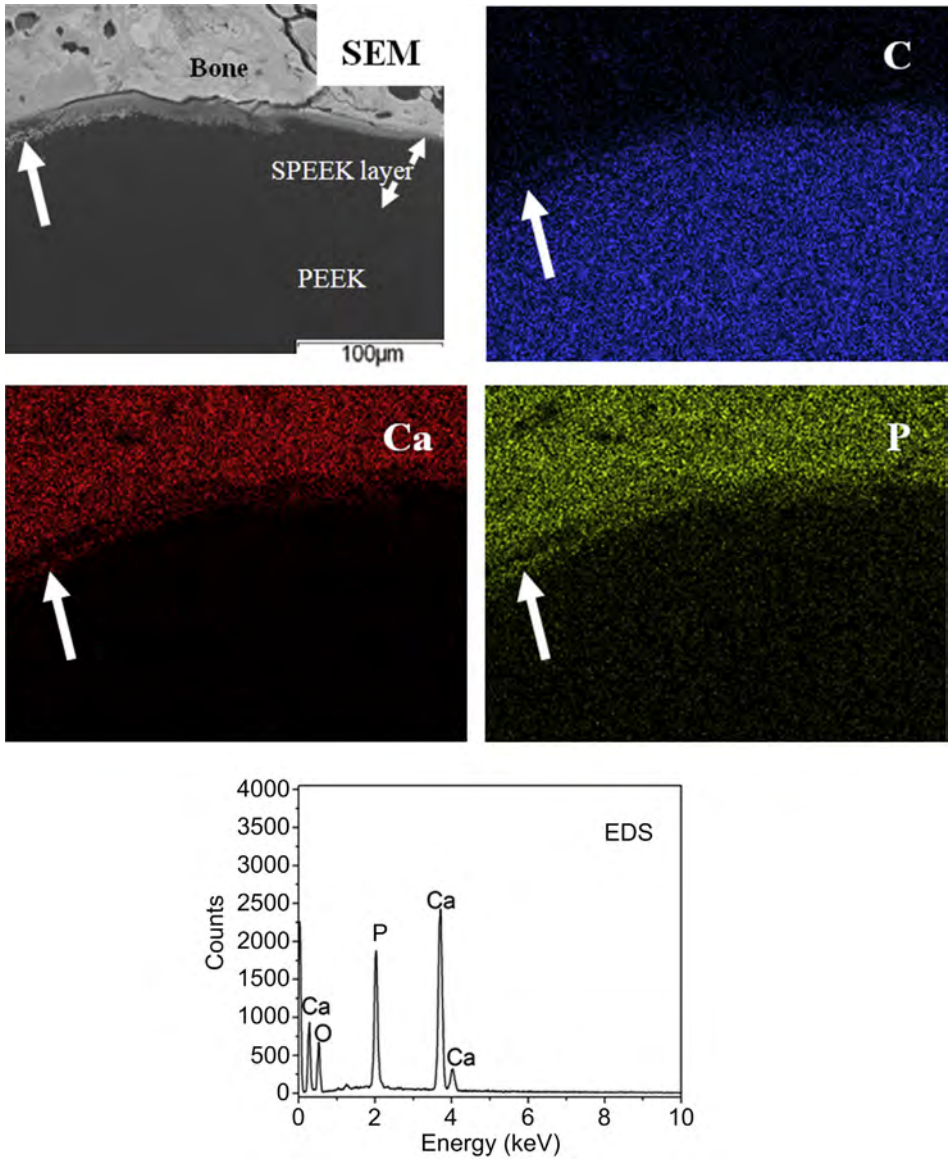

Fig. 10. Backscattered SEM image and SEM-EDS maps (C, carbon; Ca, calcium; P, phosphorous) of the implant 8 weeks after implantation and EDS analysis of newly formed bone. New bone is formed on the SPEEK surface and bonds directly. Bone ingrowth (white arrows) can be observed from the SPEEK-WA interface.

does not dissolve SPEEK [42], rinsing by acetone only removes the residual sulfuric acid in the porous network but does not alter the chemical composition and surface morphology. Hence, SPEEK-WA and SPEEK-W are very similar except the local *pH* environment. In addition, the water contact angle is significantly increased after sulfonation even though hydrophilic SO_3H groups are introduced to the surface. It implies that the surface morphology with the 3D porous and nanostructured network plays a key role in decreasing the surface hydrophilicity. Our data confirm the variation in the surface chemistry before and after sulfonation. The SO_3H groups as the dominant groups together with porous structure exert positive effects on pre-osteoblast functions according to the *in vitro* results, indicating good biocompatibility and safety. It is consistent with Sundar's [43] observation from SPEEK beads.

However, SPEEK-W and SPEEK-WA exhibit different cytocompatibility. Compared to SPEEK-W, SPEEK-WA offers a more favorable cell environment for cell adhesion and proliferation. It is likely caused by the local pH variation. As shown in the XPS and FTIR spectra (Fig. 3), there are more sulfur-containing groups on SPEEK-W than SPEEK-WA. The extra sulfur-containing groups on SPEEK-W stem from the residual sulfuric acid. Since cell adhesion and proliferation tend to be suppressed at a low pH environment [44], SPEEK-W shows lower cytocompatibility than SPEEK-WA. It should be noted that the cytocompatibility of SPEEK-W is still superior to that of the PEEK control despite the residual sulfuric acid. Here, acetone is a key reagent to reduce the amount of residual sulfuric acid from the porous network without changing the morphology and chemical composition of SPEEK. In addition, the percentage of apoptotic cells and necrotic cells on SPEEK-WA does not increase compared to SPEEK-W and PEEK control. It indicates that there are no obvious negative effects on the cells due to acetone rising.

Since the *in vitro* and *in vivo* performance of biomaterials is often different, it is necessary to conduct experiments *in vivo*. In this work, the osteoconductivity is evaluated using the rat model. One week after surgery, more than 10% decrease in the bone volume is found on SPEEK-W. The decrease in bone volume may be ascribed to the residual sulfuric acid in the porous SPEEK-W and it correlates

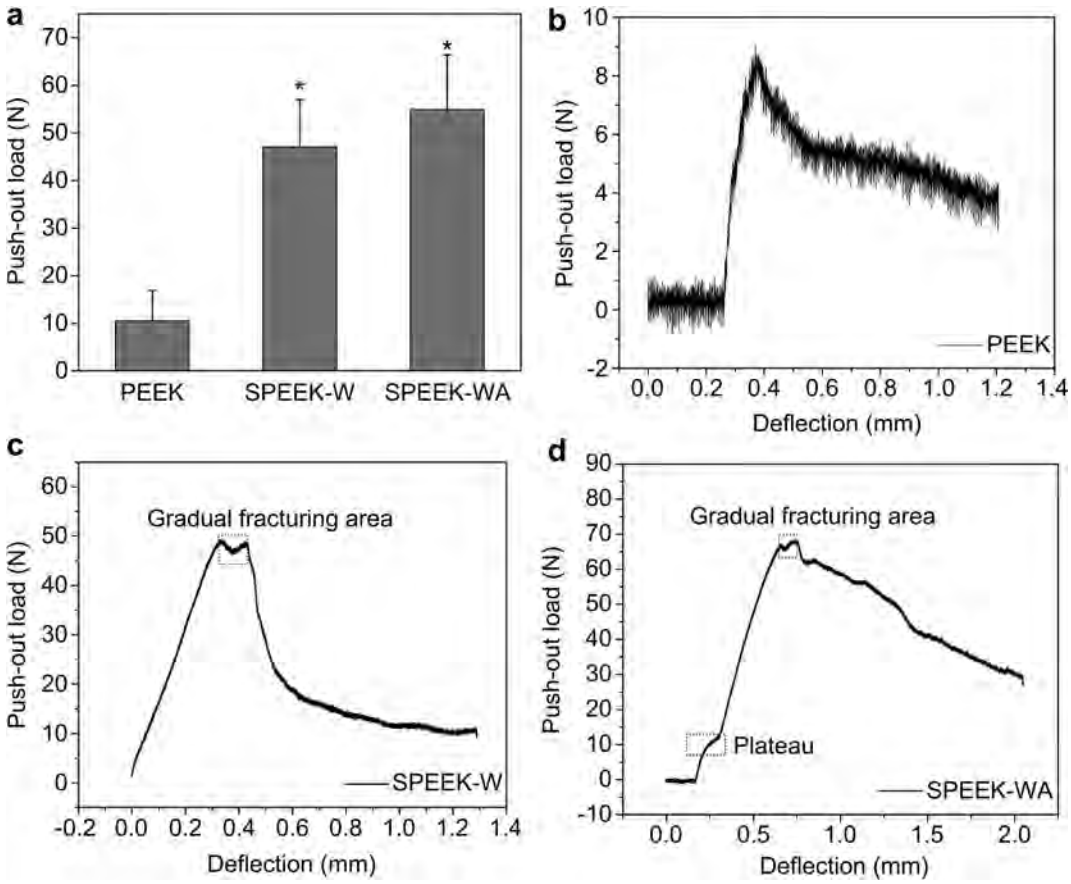

Fig. 11. Biomechanical properties measured after implantation in femur of the rats for 8 weeks: (a) Average maximum push-out load of the implants. The data are shown as mean ± standard deviation ($n = 6$) and statistical significance is indicated by $^*P < 0.05$ compared to the PEEK control; Load-deflection curves of (b) PEEK, (c) SPEEK-W, and (d) SPEEK-WA implants.

with the *in vitro* cytocompatibility results in this study. When SPEEK-W is in contact with bone marrow after implantation, the residual sulfuric acid is released. The low pH environment unavoidably inhibits the growth of osteoblasts and gives rise to slower bone formation. After 2 weeks, the bone volume on SPEEK-W increases slightly, possibly due to the reduced residual sulfuric acid on the implant through diffusion and absorption. However, the bone volume is not increased continuously during the following time and is lower than that on the PEEK control throughout the whole implantation period. The reason is not clear and more studies are required. However, it is obvious that a low pH has a strong influence on the *in vivo* bone formation on SPEEK-W. Different from SPEEK-W, the rate of new bone formation on SPEEK-WA increases continuously. The results correlate with the enhanced osteoblastic differentiation which produces a stimulatory effect on the growth of new bone tissues [45]. The result is closely correlated with osteoblast proliferation as well. Our results provide unequivocal proof that the formation of SPEEK-WA benefits the enhancement of *in vitro* and *in vivo* biocompatibility. In addition, degradation of SPEEK cannot be observed during the whole implantation period and the stability of SPEEK is crucial to clinical applications. Histological analyses reveal that the percentage of bone-implant contact on the SPEEK-WA implant is higher than those on SPEEK-W and PEEK control and the results are consistent with those obtained by the micro-CT analysis. The data indicate that for a large bone volume, the bone-implant contact increases. Additionally, obvious bone ingrowth is found from the SPEEK-WA implant thus providing valid information that the porous implant surface is anchored well with bones. Moreover, no inflammation or necrosis is observed on both SPEEK and PEEK, suggesting that the implants do not produce observable toxic effects in the surrounding tissues although a longer time point is necessary prior to clinical acceptance and fathom the healing process.

The push-out tests provide evidence that the 3D porous surface structure enables high level of mechanical interlocking between the implant and bone. Histological results indicate that the newly formed bone tissues penetrate into the porous surface layer and bond to the porous network of SPEEK, thus producing strong enough holding force to sustain the implant. Consequently, gradual fracturing takes place at the main peak during the test of porous SPEEK, whereas fractures of PEEK with smooth interfaces occur abruptly. In addition, different load progression can be observed from the load-deflection curve of SPEEK-WA and SPEEK-W in spite of similar porous structure. The results suggest that the progress of the push-out force of SPEEK-WA is hindered due to stronger bonding at the implant–bone interface compared to SPEEK-W. It is consistent with the histological analysis. The load-deflection curve of SPEEK-WA shows a typical plateau related to the collapse of cells in the initial stage of loading, implying that there are more osteoblasts around the implant *in vivo*. They are believed to be the reasons why SPEEK-WA is better for fast bone ingrowth and osseointegration than SPEEK-W. The good osseointegration subsequently improves the bonding strength [27]. In this study, the porous SPEEK-WA implant has the largest bonding strength indicating it possess the superior ability to bond with host bones thereby boding well application to orthopedic implants.

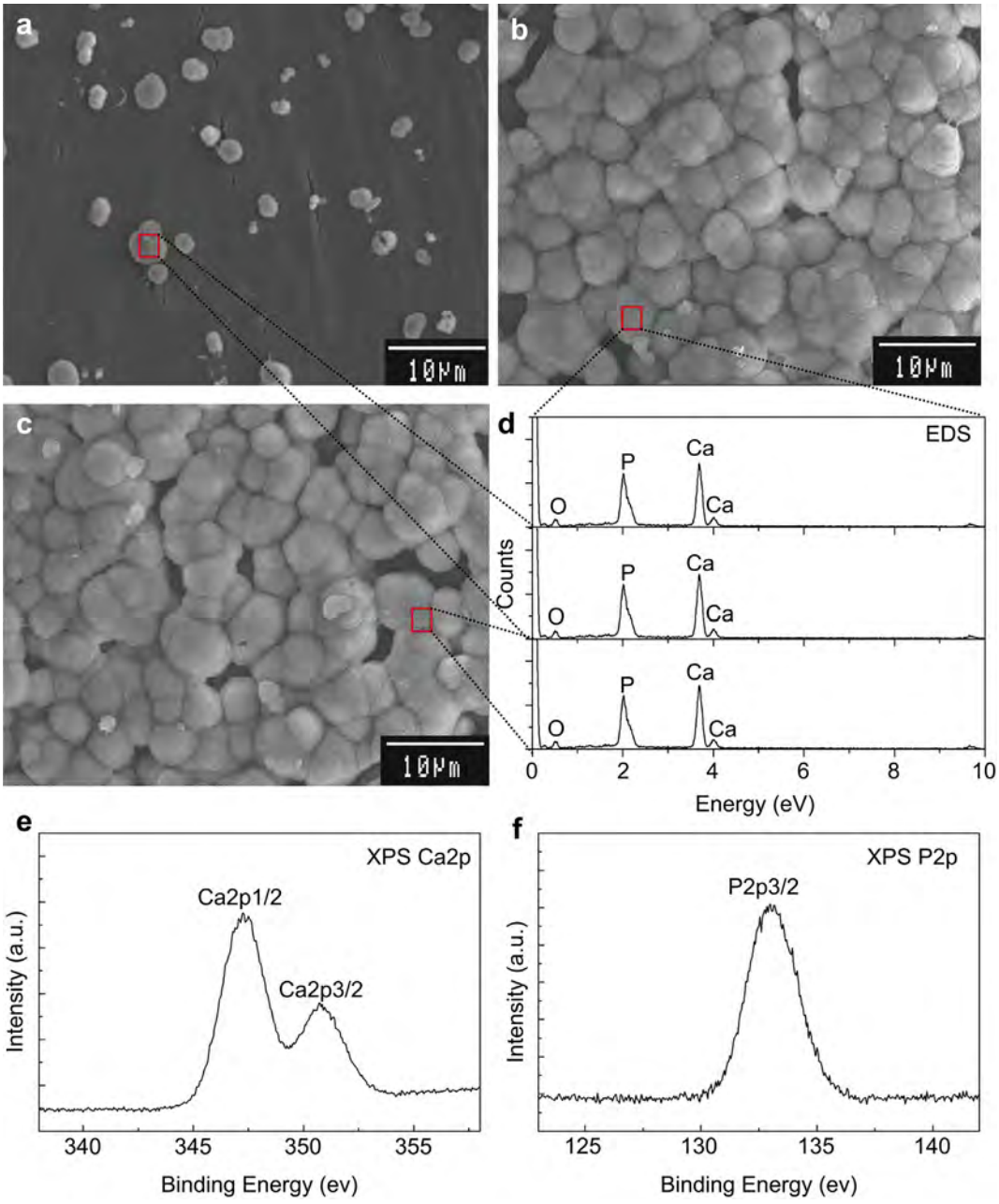

Fig. 12. SEM photographs acquired from (a) PEEK, (b) SPEEK-W, (c) SPEEK-WA sample soaked in SBF for 28 days. (d) EDS spectra. (e,f) XPS Ca2P and P2p spectra of SPEEK-WA sample soaked in SBF for 28 days.

In addition to the biocompatibility enhancement, sulfonation can induce apatite formation. The mechanism can be explained in terms of the electrostatic interaction of the functional groups with the ions in the SBF. In a completely dry environment, it is assumed that the net charge of the SO_3H groups is zero [46]. In an aqueous medium, the neutral SO_3H group will dissociate into SO_3^- and H^+ *via* proton transfer (Fig. S2, Step 1) and hence, the SPEEK surface after immersion in SBF is negatively charged. Previous studies show that the SBF can induce heterogeneous nucleation and growth of apatite while in contact with foreign surfaces. Considering the ionic nature, the electrostatic interaction triggers initial nucleation. Consequently, positively-charged calcium ions (Ca^{2+}) in the SBF are first incorporated to the surfaces (Fig. S2, Step 2). As the Ca^{2+} ions accumulate, the surface gradually gains an overall positive charge

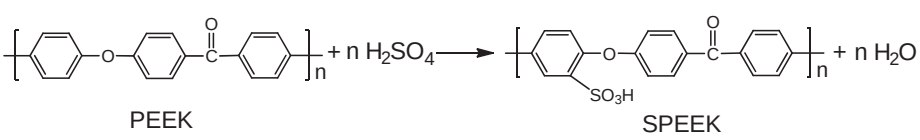

Scheme 1. Sulfonation of PEEK.

and selectively attracts negatively-charged phosphate ions (HPO_4^{2-}), leading to the formation of a hydrated precursor cluster consisting of calcium hydrogen phosphate [47] (Fig. S2, Step 3 and 4). Since this phase is metastable, it grows spontaneously and transform into stable bone-like apatite crystals by consuming Ca^{2+}, HPO_4^{2-} and OH^- ions from SBF (Fig. S2, Step 5). Our data disclose that the bioactivity on SPEEK-WA and SPEEK-W is better than that on the PEEK control. The bioactive SO_3H groups are believed to the main reason of apatite-forming ability enhancement.

5. Conclusion

Sulfonation and subsequent water immersion are utilized to produce a three-dimensional porous and nanostructured network on PEEK. After further treatment with acetone, the surface-modified PEEK sample (SPEEK-WA) exhibits remarkably improved bioactivity, cytocompatibility, osseointegration, and bone-implant bonding strength both *in vitro* and *in vivo* due to the effects of the porous structure and SO_3H functional groups. The surface treatment process described here is simple, inexpensive, and industrially scalable and the modified PEEK materials with the stable 3D surface structure are suitable for orthopedic implants.

Acknowledgments

This work was jointly supported by HKU Seed Funding for Basic Research, Hong Kong Research Grant Council (RGC) General Research Funds (GRF) #719411 and #112212, and City University of Hong Kong Applied Research Grants 9667066.

Appendix A. Supplementary data

Supplementary data related to this article can be found at http://dx.doi.org/10.1016/j.biomaterials.2013.08.071.

References

[1] Liu XY, Chu PK, Ding CX. Surface modification of titanium, titanium alloys, and related materials for biomedical applications. Mater Sci Eng R 2004;47:49–121.
[2] Sagomonyants KB, Smith MLJ, Devine JN, Aronow MS, Gronowicz GA. The in vitro response of human osteoblasts to polyetheretherketone (PEEK) substrates compared to commercially pure titanium. Biomaterials 2008;29:1563–72.
[3] Kurtz SM, Devine JN. PEEK biomaterials in trauma, orthopedic, and spinal implants. Biomaterials 2007;28:4845–69.
[4] Williams D. Polyetheretherketone for long-term implantable devices. Med Device Technol 2008;19(1):8–11.
[5] Toth JM, Wang M, Estes BT, Scifert JL, Seim III HB, Turner AS. Polyetheretherketone as a biomaterial for spinal applications. Biomaterials 2006;27:324–34.
[6] Xing P, Robertson GP, Guiver MD, Mikhailenko SD, Wang K, Kaliaguine S. Synthesis and characterization of sulfonated poly(ether ether ketone) for proton exchange membranes. J Memb Sci 2004;229:95–106.
[7] Sobieraj MC, Kurt SM, Rimnac CM. Notch sensitivity of PEEK in monotonic tension. Biomaterials 2009;30:6485–94.
[8] Han CM, Lee EJ, Kim HE, Koh YH, Kim KN, Ha Y, et al. The electron beam deposition of titanium on polyetheretherketone (PEEK) and the resulting enhanced biological properties. Biomaterials 2010;31:3465–70.
[9] Barton AJ, Sagers RD, Pitt WG. Bacterial adhesion to orthopaedic implant polymers. J Biomed Mater Res 1996;30:403–10.
[10] Yu S, Hariram KP, Kumar R, Cheang P, Aik KK. In vitro apatite formation and its growth kinetics on hydroxyapatite/polyetheretherketone biocomposites. Biomaterials 2005;26:2343–52.
[11] Abu Bakar MS, Cheng MHW, Tang SM, Yu SC, Liao K, Tan CT, et al. Tensile properties, tension-tension fatigue and biological response of polyetheretherketone-hydroxyapatite composites for load-bearing orthopedic implants. Biomaterials 2003;24:2245–50.
[12] Wong KL, Wong CT, Liu WC, Pan HB, Fong MK, Lam WM, et al. Mechanical properties and in vitro response of strontium-containing hydroxyapatite/polyetheretherketone composites. Biomaterials 2009;30:3810–7.
[13] Converse GL, Conrad TL, Merrill CH, Roeder RK. Hydroxyapatite whisker-reinforced polyetherketoneketone bone ingrowth scaffolds. Acta Biomater 2010;6:856–63.
[14] Converse GL, Yue W, Roeder RK. Processing and tensile properties of hydroxyapatite-whisker-reinforced polyetheretherketone. Biomaterials 2007;28:927–35.
[15] Fan JP, Tsui CP, Tang CY, Chow CL. Influence of interphase layer on the overall elasto-plastic behaviors of HA/PEEK biocomposite. Biomaterials 2004;25:5363–73.
[16] Bobyn JD, Stackpool GJ, Hacking SA, Tanzer M, Krygier JJ. Characteristics of bone ingrowth and interface mechanics of a new porous tantalum biomaterial. J Bone Jt Surg Br 1999;81-B:907–14.
[17] Karageorgiou V, Kaplan D. Porosity of 3D biomaterial scaffolds and osteogenesis. Biomaterials 2005;26:5474–91.
[18] Kobayashi T, Rikukawa M, Sanui K, Ogata N. Proton-conducting polymers derived from poly(ether-etherketone) and poly(4-phenoxybenzoyl-1,4-phenylene). Solid State Ionics 1998;106:219–25.
[19] Chu PP, Wu CS, Liu PC, Wang TH, Pan JP. Proton exchange membrane bearing entangled structure: sulfonated poly (ether ether ketone)/bismaleimide hyperbranch. Polymer 2010;51:1386–94.
[20] Hickner MA, Ghassemi H, Kim YS, Einsla BR, McGrath JE. Alternative polymer systems for proton exchange membranes (PEMs). Chem Rev 2004;104:4587–612.
[21] Zhao Y, Wong SM, Wong HM, Wu S, Hu T, Yeung KWK, et al. Effects of carbon and nitrogen plasma immersion ion implantation on in vitro and in vivo biocompatibility of titanium alloy. ACS Appl Mater Interfaces 2013;5:1510–6.
[22] Kokubo T, Kim HM, Kawashita M. Novel bioactive materials with different mechanical properties. Biomaterials 2003;24:2161–75.
[23] Nasaf MM, Saidi H. Surface studies of radiation grafted sulfonic acid membranes: XPS and SEM analysis. Appl Surf Sci 2006;252:3073–84.
[24] Pino M, Stingelin N, Tanner KE. Nucleation and growth of apatite on NaOH-treated PEEK, HDPE and UHMWPE for artificial cornea materials. Acta Biomater 2008;4:1827–36.
[25] Infrared spectroscopy: IR absorptions for representative functional groups. Available from: http://www.chemistry.ccsu.edu/glagovich/teaching/316/ir/table.html; 2013.
[26] Doğan H, Inan TY, Koral M, Kaya M. Organo-montmorillonites and sulfonated PEEK nanocomposite membranes for fuel cell applications. Appl Clay Sci 2011;52:285–94.
[27] Liu X, Wu S, Yeung KWK, Chan YL, Hu T, Xu Z, et al. Relationship between osseointegration and superelastic biomechanic in porous NiTi scaffold. Biomaterials 2011;32:330–8.
[28] Song WH, Jun YK, Han Y, Hong SH. Biomimetic apatite coatings on micro-arc oxidized titania. Biomaterials 2004;25:3341–9.
[29] Ku Y, Chung CP, Jang JH. The effect of the surface modification of titanium using a recombinant fragment of fibronectin and vitronectin on cell behavior. Biomaterials 2005;26:5153–7.
[30] Williams DF. On the mechanisms of biocompatibility. Biomaterials 2008;29:2941–53.
[31] Zhao Y, Wu G, Jiang J, Wong HM, Yeung KWK, Chu PK. Improved corrosion resistance and cytocompatibility of magnesium alloy by two-stage cooling in thermal treatment. Corros Sci 2012;59:360–5.
[32] Zhao L, Mei S, Chu PK, Zhang Y, Wu Z. The influence of hierarchical hybrid micro/nano-textured titanium surface with titania nanotubes on osteoblast functions. Biomaterials 2010;31:5072–82.
[33] Tachibana A, Kaneko S, Tanabe T, Yamauchi K. Rapid fabrication of keratin-hydroxyapatite hybrid sponges toward osteoblast cultivation and differentiation. Biomaterials 2005;26:297–302.
[34] Yamaguchi A, Komori T, Suda T. Regulation of osteoblast differentiation mediated by bone morphogenetic proteins, hedgehogs, and Cbfa1. Endocr Rev 2000;21:393–411.
[35] Khang D, Choi J, Im YM, Kim YJ, Jang JH, Kan SS, et al. Role of subnano-, nano- and submicron-surface features on osteoblast differentiation of bone marrow mesenchymal stem cells. Biomaterials 2012;26:5998–6007.
[36] Kunzler TP, Drobek T, Schuler M, Spencer ND. Systematic study of osteoblast and fibroblast response to roughness by means of surface-morphology gradients. Biomaterials 2007;28:2175–82.
[37] Chu PK, Chen JY, Wang LP, Huang N. Plasma surface modification of biomaterials. Mater Sci Eng R 2002;36:143–206.
[38] Wu L, Ding J. Effects of porosity and pore size on in vitro degradation of three-dimensional porous poly(D, L-lactide-co-glycolide) scaffolds for tissue engineering. J Biomed Mater Res A 2005;75:767–77.
[39] Guldberg RE, Duvall CL, Peister A, Oest ME, Lin ASP, Palmer AW, et al. 3D imaging of tissue integration with porous biomaterials. Biomaterials 2008;29:3757–61.
[40] Daoust D, Devaux J, Godard P. Mechanism and kinetics of poly(ether ether ketone) (PEEK) sulfonation in concentrated sulfuric acid at room temperature. Part 1. Qualitative comparison between polymer and monomer model compound sulfonation. Polym Int 2001;50:917–24.
[41] Zaidi SMJ, Mikhailenko SD, Robertson GP, Guiver MD, Kaliaguine S. Proton conducting composite membranes from polyether ether ketone and heteropolyacids for fuel cell applications. J Memb Sci 2000;173:17–34.
[42] Wu HL, Ma CCM, Li CH, Chen CY. Swelling behavior and solubility parameter of sulfonated poly(ether ether ketone). J Polym Sci Part B Polym Phys 2006;44:3128–34.

[43] Sundar SS, Sangeetha D. Investigation on sulphonated PEEK beads for drug delivery, bioactivity and tissue engineering applications. J Mater Sci 2012;47:2736–42.
[44] Shen YH, Liu WC, Wen CY, Pan HB, Wang T, Darvell BW, et al. Bone regeneration: importance of local pH–strontium-doped borosilicate scaffold. J Mater Chem 2012;22:8662–70.
[45] Witte F, Kaese V, Haferkamp H, Switzer E. In vivo corrosion of four magnesium alloys and the associated bone response. Biomaterials 2005;26:3557–63.
[46] Wihelm M, Jeske M, Marschall R, Cavalcanti WL, Tölle P, Köhler C, et al. New proton conducting hybrid membranes for HT-PEMFC systems based on polysiloxanes and SO_3H-functionalized mesoporous Si-MCM-41 particles. J Memb Sci 2008;316:164–75.
[47] Wang HY, Ji JH, Zhang W, Zhang YH, Jiang J, Wu ZW, et al. Biocompatibility and bioactivity of plasma-treated biodegradable poly(butylenes succinate). Acta Biomater 2009;5:279–87.

Supporting Information

Cytocompatibility, osseointegration, and bioactivity of three-dimensional porous and nanostructured network on polyetheretherketone (PEEK)

Ying Zhao [a,b,1], Hoi Man Wong [a,1], Wenhao Wang [a,b], Penghui Li [b], Zushun Xu [c], Eva Y.W. Chong [a], Chun Hoi Yan [a], Kelvin W. K. Yeung [a,d*], Paul K. Chu [b,**]

[a] *Department of Orthopaedics & Traumatology, The University of Hong Kong, Pokfulam Road, Hong Kong, China*

[b] *Department of Physics and Materials Science, City University of Hong Kong, Tat Chee Avenue, Kowloon, Hong Kong, China*

[c] *Ministry-of-Education Key Laboratory for the Green Preparation and Application of Functional Materials, College of Materials Science and Engineering, Hubei University, Wuhan 430062, China*

[d] *Shenzhen Key Laboratory for Innovative Technology in Orthopaedic Trauma, The University of Hong Kong Shenzhen Hospital, 1 Haiyuan 1st Road, Futian Distract, Shenzhen, China*

[*] Corresponding author. Tel.: +852 22554654; Fax: +852 28174392.
[**] Corresponding author. Tel.: +852 34427724; Fax: +852 34420542.
E-mail: wkkyeung@hku.hk (K. W. K. Yeung), paul.chu@cityu.edu.hk (P. K. Chu)
[1] The authors share the co-first authorship.

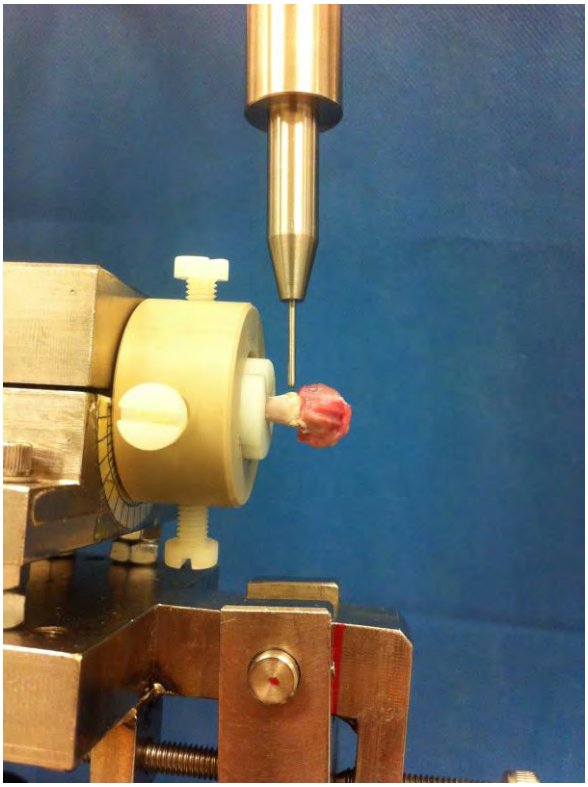

Figure S1. Biomechanical test apparatus for push-out tests.

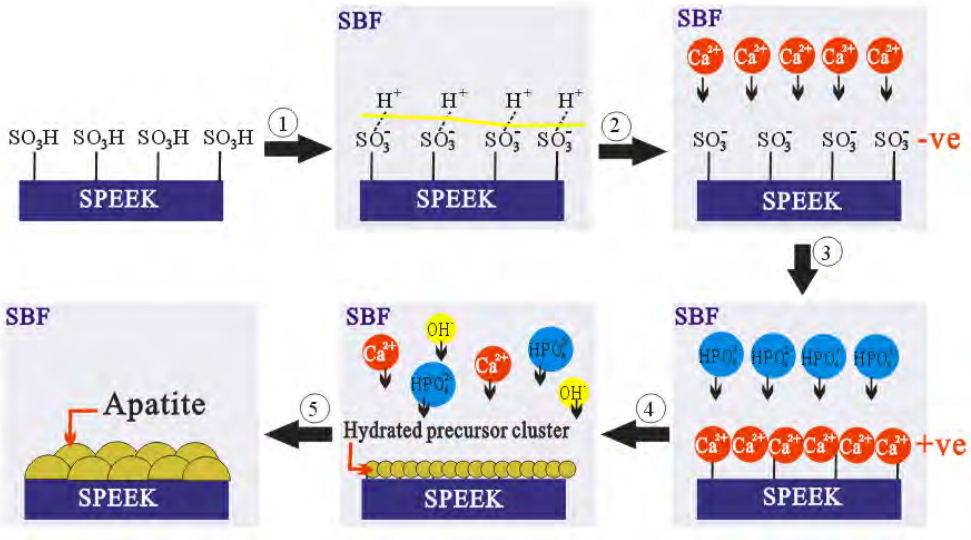

Figure S2. Schematic diagram of the apatite formation on the surface of the 3D porous SPEEK samples.